ResearchGate

See discussions, stats, and author profiles for this publication at: https://www.researchgate.net/publication/256477374

Ultrafast Electron Transfer and Trapping Dynamics in the Interband- gap States of ZrO2 Nanoparticles Sensitized by Baicalein (BIC)

ARTICLE *in* THE JOURNAL OF PHYSICAL CHEMISTRY C · AUGUST 2013

Impact Factor: 4.77 · DOI: 10.1021/jp403473h

CITATIONS
6

READS
102

5 AUTHORS, INCLUDING:

Partha Maity
Bhabha Atomic Research Centre
17 PUBLICATIONS **54** CITATIONS
SEE PROFILE

Tushar Debnath
Department of Atomic Energy
17 PUBLICATIONS **54** CITATIONS
SEE PROFILE

Arshad Akbar
Indian Institute of Science Education and Res…
2 PUBLICATIONS **6** CITATIONS
SEE PROFILE

Hirendra N Ghosh
Bhabha Atomic Research Centre
127 PUBLICATIONS **3,814** CITATIONS
SEE PROFILE

Available from: Tushar Debnath
Retrieved on: 17 January 2016

THE JOURNAL OF PHYSICAL CHEMISTRY C

Article

pubs.acs.org/JPCC

Ultrafast Electron-Transfer and -Trapping Dynamics in the Inter-Band-Gap States of ZrO_2 Nanoparticles Sensitized by Baicalein

Partha Maity, Tushar Debnath, Arshad Akbar, Sandeep Verma, and Hirendra N. Ghosh*

Radiation & Photochemistry Division, Bhabha Atomic Research Center, Trombay, Mumbai 400 085, India

Supporting Information

ABSTRACT: Charge-transfer dynamics of baicalein (BIC) adsorbed on TiO_2 and ZrO_2 nanoparticles have been studied by steady-state and time-resolved emission spectroscopy and femtosecond transient absorption spectroscopy. Steady-state absorption and emission studies indicate that the BIC molecule forms a charge-transfer (CT) complex with both TiO_2 and ZrO_2 nanoparticles through its pyrogallol moiety and quinone moiety, respectively. On exciting the CT complex a new charge-transfer emission band was detected only in the BIC−ZrO_2 system not from the BIC−TiO_2 system. On photoexcitation of BIC−TiO_2 and BIC−ZrO_2 systems by an ultrafast laser pulse, electron injection into the nanoparticles has been confirmed for both systems by direct detection of the electron in the nanoparticle and cation radical of BIC ($BIC^{\bullet+}$) in the transient spectra. Ultrafast transient decay kinetics of the $BIC^{\bullet+}$ cation radical suggests that back electron transfer (ET) dynamics is multiexponential on both nanoparticle surfaces. Due to the fact that the first excited state (S_1) state lies below the conduction band edge of ZrO_2, our measurements suggest that in the case of ZrO_2 electrons are directly injected into the surface states and getting trapped in different surface states with a time constant of 900 fs before slow recombination with BIC cation radical. From the above investigation we suggest that electron injection into the surface states of nanoparticles is only feasible or facilitated when the adsorbate forms a strong CT complex with the nanoparticles.

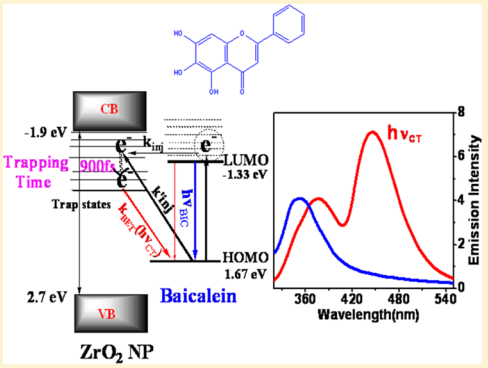

1. INTRODUCTION

Interfacial electron transfer plays a major role in several physical and physico-chemical processes.[1−4] Interest in this field has grown daily due to diverse applications like photocatalysis, photovoltaics, molecular electronics, etc.[5−7] One of the main applications is development of dye-sensitized solar cells (DSSCs), which has emerged as a promising class of photovoltaic device with potential of low-cost production.[8−10] The highest efficiency of DSSC was reported to be 12.3% employing a mesoporous TiO_2 electrode cosensitized with Zn−porphyrin and cyclopentadithiophene dyes and a cobalt(II/III)-based redox electrolyte.[11,12] The basic photophysical process in a solar cell device is electron injection from the electronically excited state of the adsorbed dye into the conduction band of the nanoparticle, which takes place on a fast and an ultrafast time scale.[13−26]

In dye−semiconductor nanoparticle systems electron injection is in competition with both emissions of the excited state of the dye and a radiationless transition to the ground state. In addition, the excited state can also inject an electron in the inter-band-gap states of nanoparticles.[27−32] The electron injected in the nanoparticles can either diffuse to the electrode, which is part of the electrical circuit, or undergo a deleterious energy wasteful step such as recombining with the dye cation. It is a well-accepted phenomenon that once the electrons are moved or injected into the defect states they cannot be used any more for the energy conversion process. However, very recently, Greenwald et al.[33] reported CdSe quantum dot solar cell based on a porous ZrO_2 film where they have indicated electron injection from a photoexcited quantum dot into a ZrO_2 film which is unexpected due to the much higher conduction band edge (closer to the vacuum level) of bulk ZrO_2 as compared to TiO_2. This observation clearly indicates in many systems where the photoexcited energy level of sensitizers lies below the conduction band, still electron injection takes place in the inter-band-gap states and also can contribute to conversion of solar energy.

A majority of the investigations on interfacial ET dynamics discuss electron injection into the conduction band of a semiconductor as most of the sensitizer has a LUMO level higher than that of the conduction band of TiO_2 nanoparticles. Over the years it has been realized that inter-band-gap states play an important and active role in the interfacial electron-transfer dynamics in dye-sensitized semiconductor nanoparticles. However, reports are available mostly for injection to the conduction band (high density of states) of the nanoparticles.[13−26] Nevertheless, Huber et al.[27] and we[28−32] reported electron injection into the surface states of wide-band-gap (E_g > 4.5 eV) semiconductor ZrO_2 sensitized by alizarin,[27] quinizarin,[28,29] quinizarin derivatives,[30] and osmium polypyridyl

Received: April 9, 2013
Revised: July 31, 2013
Published: August 2, 2013

 © 2013 American Chemical Society

complex[31] and ZnS sensitized by quinizarin.[32] In all the wide-band-gap semiconductors the electrons are injected into the surface states and can be easily trapped depending upon the trapped depth. It is very important to have knowledge of trapping dynamics before charge recombination with the parent cation. Theoretical studies have indicated that BET dynamics in dye-sensitized nanoparticles is often controlled by trapping, detrapping, and delocalization dynamics of the injected electrons.[34,35] In all the earlier experimental studies charge-transfer dynamics on ZrO_2 nanoparticles were carried out by exciting the sensitizer, where the photoexcited (S_1) state injects an electron into the surface states. In those studies it was difficult to monitor only ET dynamics into the surface states as the excited states of the sensitizers show transient absorption in the same spectral region where both electron and cation radicals have transient absorption. Thus, it is very important to study interfacial ET dynamics on a wide-band-gap semiconductor (ZrO_2) where excited dynamics of the adsorbate does not interfere with ET dynamics (both electron injection and back ET).

In the present studies we are reporting the interfacial electron-transfer dynamics of baicalein-sensitized ZrO_2 and TiO_2 nanoparticles where baicalein (BIC) forms a charge-transfer (CT) complex through the quinonoid and catecholate moieties, respectively. Here we chose the TiO_2 nanoparticle to compare the ET dynamics with smaller band-gap materials. Charge-transfer luminescence was detected only in the BIC−ZrO_2 system. Electron injection in both nanoparticles has been confirmed by monitoring the cation radical and injected electron in the nanoparticles as detected by femtosecond transient absorption spectrometry. Cyclic voltamtery and luminescence spectroscopy studies suggest that the LUMO level of the BIC molecule lies far below the conduction band edge of ZrO_2 but well above the conduction band edge of TiO_2. However, the appearance of BIC cation radical in transient spectra suggests that electron transfer takes place in the inter-band-gap states of ZrO_2 nanoparticle. Electron injection was found to be pulsed (<100 fs), and back ET dynamics is multiexponential on both nanoparticle surfaces. Charge recombination dynamics was found to be faster on the TiO_2 nanoparticle as compared the ZrO_2 nanoparticle surface. On the ZrO_2 nanoparticle surface after injection into the surface state the electron goes for a trapping process with a time constant of 900 fs before recombining with the BIC cation radical. Our observation suggests formation of a strong CT complex facilitating electron injection into the inter-band-gap states of ZrO_2 nanoparticles.

2. EXPERIMENTAL SECTION

a. Materials. Baicalein was obtained from Aldrich and used without further purification. Titanium(IV) tetraisopropoxide {$Ti[OCH(CH_3)_2]_4$} (Aldrich, 97%), methanol (Aldrich), and isopropyl alcohol (Aldrich) were purified by distillation. Zirconium(IV) isopropoxide isopropanol complex $Zr[OCH(CH_3)_2]_4\cdot(CH_3)_2CHOH$ (Aldrich, 99.9%) was used without further purification. Nanopure water (Barnsted System, USA) was used for making aqueous solutions.

b. Sample Preparation. Nanometer-size TiO_2 was prepared by controlled hydrolysis of titanium(IV) tetraisopropoxide.[13] A solution of 5 mL of $Ti[OCH(CH_3)_2]_4$ (Aldrich, 97%) dissolved in 95 mL of isopropyl alcohol (Aldrich) was added dropwise (1 mL/min) to 900 mL of nanopure water (2 °C) at pH 1.5 (adjusted with HNO_3). The solution was continuously stirred 10−12 h until a transparent colloid was formed. The colloidal solution was concentrated at 35−40 °C with a rotary evaporator and then dried with a nitrogen stream to yield a white powder. Again, ZrO_2 nanoparticles in aqueous solution were prepared by controlled hydrolysis of zirconium(IV) tetraisopropoxide. In brief, 5 mmol (1.94 g) of $Zr[OCH(CH_3)_2]_4\cdot(CH_3)_2CHOH$ (Aldrich, 99.9%) was dissolved in ∼100 mL of isopropyl alcohol (Aldrich) after vigorous stirring and added dropwise (1 mL/min) to ∼900 mL of nanopure water at pH 2 (adjusted using conc HNO_3) with rigorous stirring in about 1 h at 0−2 °C. Stirring was continued for 2 h at that temperature and then at room temperature overnight. The solution was concentrated at 40−50 °C using a rotary evaporator and then finally dried to yield a fine white powder. High-resolution TEM images have been recorded for the newly synthesized ZrO_2 nanoparticles where size was found to be ∼4 nm and are reported in the Supporting Information. In the present work all colloidal samples were prepared after dispersing the dry TiO_2 or ZrO_2 nanoparticles in water (15g/L). A transparent clear colloidal solution was formed. BIC is sparingly soluble in water; however, solubility increases dramatically in the presence of both TiO_2 and ZrO_2 nanoparticles. This observation clearly indicates that interactions between BIC and TiO_2/ZrO_2 nanoparticles are quite strong. For all our sensitization experiments we added BIC molecules in TiO_2 and ZrO_2 colloidal solution and sonicated a couple of minutes till we got a clear transparent solution. For the entire measurements sample solutions were deoxygenated by continuously bubbling high-purity nitrogen (99.95 Iolar grade from Indian Oxygen Co. Ltd., India) through the solutions. For ultrafast transient absorption studies the solutions were flowed through a 1 mm path quartz cell during all measurements.

c. Femtosecond Transient Absorption Studies. A femtosecond tunable visible spectrometer has been developed based on a multipass amplified femtosecond Ti:sapphire laser system supplied by Thales, France. Pulses of 20 fs duration and 4 nJ energy per pulse at 800 nm obtained from a self-mode-locked Ti-Sapphire laser oscillator (Synergy 20, Femtolaser, Austria) were amplified in a regenerative and two-pass amplifier pumped by a 20W DPSS laser (Jade) to generate 40 fs laser pulses of about 1.2 mJ energy at a repetition rate of 1 kHz. The 800 nm output pulse from the multipass amplifier is split into two parts to generate pump and probe pulses. In the present investigation we used frequency doubled 400 nm as excitation sources. To generate pump pulses at 400 nm one part of 800 nm with 200 μJ/pulse is frequency doubled in BBO crystals. To generate visible probe pulses, about 3 μJ of the 800 nm beam is focused onto a 1.5 mm thick sapphire window. The intensity of the 800 nm beam is adjusted by iris size and ND filters to obtain a stable white light continuum in the 400 to over 1000 nm region. Probe pulses are split into the signal and reference beams and detected by two matched photodiodes with variable gain. We kept the spot sizes of the pump beam and probe beam at the crossing point around 500 and 300 μm, respectively. The noise level of the white light is about ∼0.5% with occasional spikes due to oscillator fluctuation. We noticed that most laser noise is low-frequency noise and can be eliminated by comparing the adjacent probe laser pulses (pump blocked vs unblocked using a mechanical chopper). The typical noise in the measured absorbance change is about <0.3%. The instrument response function (IRF) for 400 nm excitation was obtained by fitting the rise time of the bleaching of the

sodium salt of *meso*-tetrakis(4-sulfonatophenyl)porphyrin (TPPS) at 710 nm and was found to be 120 fs.[36] All samples were dissolved in nanopure water. The experimental solution was circulated to avoid sample bleaching during the course of the experiment. Data analysis and fitting at individual wavelengths were carried out by the Lab-View program.

d. Cyclic Voltammetry. Voltammetric experiments were performed with Auto Lab PGSTAT 20 (Manufactured by Eco-Chemie, Netharlands) coupled to a Metrohm 663 VA stand electrode system comprising of glassy carbon (GC)/Pt/Ag/AgCl. The PG STAT was driven by Autolab software. The temperature of the solution was maintained at 25 ± 0.1 °C. Measurements were done in acetonitrile solution with TBAHP (tetrabutylammonium hexafluorophosphate) as a supporting electrolyte and in N_2 atmosphere. The redox potential of the BIC molecule has been determined to be 1.45 V against Ag/AgCl electrode.

e. Steady-State Optical Absorption and Emission Spectrometer. Steady-state absorption spectra were recorded on a Thermo-Electron model Biomate spectrophotometer. Fluorescence spectra, which were corrected for the wavelength dependence of the instrument sensitivity, were recorded using a Hitachi model 4010 Spectrofluorometer.

f. Time-Resolved Emission Spectrometer. Time-resolved fluorescence measurements were carried out using a diode laser-based spectrofluorimeter from IBH (UK). The instrument works on the principle of time-correlated single-photon counting (TCSPC). In the present work, 280, 374, and 405 nm laser pulses were used as the excitation light sources and a TBX4 detection module (IBH) coupled with a special Hamamatsu PMT was used for fluorescence detection.

3. RESULTS AND DISCUSSION

a. Dye Binding and Formation of Charge-Transfer Complex. The main aim of this investigation is to monitor electron-transfer processes in the mid-band-gap states of a wide-band-gap semiconductor. We observed in our earlier studies that it is a prerequisite condition for electron injection in the surface states (inter-band-gap states) of a wide-band semiconductor, where dye and semiconductor nanoparticles have to interact very strongly in the ground state with formation of a charge-transfer complex.[28−32] We carried out steady-state absorption measurements of baicalein molecules in ZrO_2 colloidal solutions. Figure 1 shows the optical absorption of free BIC in water and also those adsorbed on the ZrO_2 nanoparticles. The absorption maxima of the optical absorption spectra of BIC in water at pH 2.5 appear at 273 and 323 nm. However, upon addition of ZrO_2 nanoparticles, the absorption spectra shifted to longer wavelengths, with the appearance of a new peak at 352 nm. The effect of increasing ZrO_2 concentration on the absorption spectrum is also shown in Figure 1. The color of the solution changes from colorless to dark yellow on addition of ZrO_2. The increment of optical absorbance and appearance of a new red-shifted absorption band indicate electronic coupling between BIC and ZrO_2 nanoparticle is very strong and can be attributed to a CT-type of interaction. This red shift in absorption studies also might be due to aggregate formation on the nanoparticle surface. We recorded optical absorption spectra of BIC in different solvents where we can get maximum solubility in that particular solvent. It is clearly seen that even at very high concentrations optical absorption spectra of BIC are unchanged (Supporting Information). This observation clearly suggests

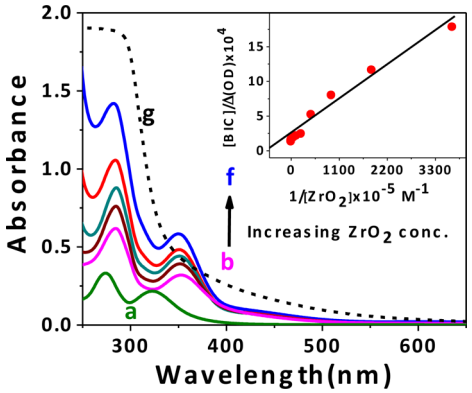

Figure 1. Absorption spectra of (a) free baicalein (56 μM) and (b−f) BIC−ZrO_2 complex. Concentrations of ZrO_2 in BIC−ZrO_2 complex are (b) 0.078, (c) 0.625, (d) 1.25, (e) 2.5, and (f) 5 g/L. (g) BIC−TiO_2 complex [TiO_2] = 0.25 g/L. (Inset) B−H plot of the BIC−ZrO_2 system.

that the possibility of aggregate formation on ZrO_2 surface is negligible. The red shift in absorption spectra of the complex is due to formation of a six-membered binding (quinol binding)[28−32] between baicalein and ZrO_2 NPs. We kept the pH of the solution ∼2.5 to avoid change of optical spectra of BIC due to pH changing. We observed that optical spectra of BIC do not change at lower pH (pH 1−6).

In our earlier investigation we observed that quinizarin (QZ), which has a keto and hydroxyl group in similar positions of BIC, forms intramolecular H bonding. However, in the presence of ZrO_2 or ZnS particles intramolecular H bonding in the Qz molecule breaks and forms a 6-membered chelate-type complex with the nanoparticle.[28−32] Similarly, we can envisage a similar 6-membered chelate-type complex between BIC and ZrO_2 nanoparticles (Scheme 1). We also observed in

Scheme 1. Molecular Structure of the Baicalein Coupled with ZrO_2 and TiO_2 Nanoparticles

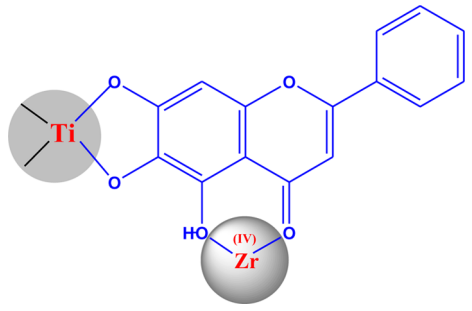

Supporting Information Figure S2 that on addition of TiO_2 nanoparticles to an aqueous solution of BIC, the optical absorption spectrum becomes broad and shifts to longer wavelength and the optical density increases. This phenomenon can also be attributed to formation of a CT complex between BIC and TiO_2. The BIC molecule has a pyrogallol moiety, i.e., three consecutive OH groups in the benzene ring, and can form a stable charge-transfer complex. Attribution of the CT complex between BIC and ZrO_2 nanoparticles has also been confirmed by steady-state emission studies, which we report in the next section. Earlier we reported that pyrogallol red (PGR) and bromo-pyrogallol red (Br−PGR), which have a pyrogallol moiety, can form a strong CT complex with TiO_2 nano-

dx.doi.org/10.1021/jp403473h | J. Phys. Chem. C 2013, 117, 17531−17539

particles.[14] Rajh et al.[37] already reported by that six-membered ring complexes are more stable on the ZrO_2 nanoparticle surface and five-membered ring complexes are more stable on the TiO_2 nanoparticle surface for <20 nm particles. It is seen in the scheme that oxygen is bonded to the central ring in the keto (quinoid) form along with one OH group binding to the Zr (IV) atom, which can sit on the surface of the nanoparticle.

Earlier formation of a CT complex between TiO_2 and ZrO_2 nanoparticle and the organic dyes[13,14,26−30] as well as inorganic molecules was observed by us and others.[21−25] Formation of a CT complex can be explained by the following equation

$$MO_2 + BIC \rightarrow [MO_2^{\delta-} \cdots BIC^{\delta+}]_{Complex} \quad (1)$$

where M is Zr and Ti.

The experimental observation can be explained in the following manner. When BIC molecules are adsorbed on the surface, a fraction of the dye molecules just get adsorbed on the surface of the nanoparticle and a major fraction of the molecules form CT complex. A modified Benesi−Hilderband equation[38] has been used to determine K_{eq} (equilibrium constant). For a CT interaction it can be represented as

$$BIC^- + \equiv M{-}OH_2^+ \xrightarrow{K_{eq}} \equiv M{-}BIC + H_2O \quad (2)$$

Since the particle concentration is proportional to the concentration of surface hydroxyl groups ($\equiv M{-}OH_2^+$), we can define the equilibrium constant as

$$K_{eq} = \frac{[M{-}BIC]}{[BIC][MO_2]} \quad (3)$$

where [BIC] is the concentration of the adsorbed dye which does not form a complex, $[MO_2]$ is the particle concentration, and [M−BIC] is the concentration of the complex. In the inset of Figure 1 we have shown the Benesi−Hilderband plot the for the BIC−ZrO_2 system. From the Benesi−Hilderband plot the equilibrium constant and molar extinction coefficient of the ZrO_2−BIC complex has been determined to be 8.06×10^6 M^{-1} and 19 230 cm^{-1} mol^{-1}, respectively. Similarly, we also determined equilibrium constant and molar extinction coefficient for the TiO_2−BIC complex from the Benesi−Hilderband plot (Supporting Information), and it was found to be 1.95×10^6 M^{-1} and 2267 cm^{-1} mol^{-1}.

b. Steady-State and Time-Resolved Emission Spectroscopy. To understand the charge-transfer behavior of BIC-sensitized ZrO_2 and TiO_2 nanoparticles it is important to understand the excited-state properties of the BIC molecule by monitoring the photoluminescence properties in the absence and presence of the nanoparticles. BIC is known to be very important molecule for its enormous biological applications;[39−41] however, detailed photoluminescence properties of BIC are not reported in the literature. Figure 2 shows the normalized emission spectra of BIC in the absence and presence of different concentration of ZrO_2 nanoparticles. Emission spectra of pure BIC show an emission band with a peak at 355 nm with low quantum yield (ϕ_f = 0.045) (Figure 2a). However, in the presence of ZrO_2 nanoparticles emission spectra changes with increasing ZrO_2 nanoparticle and we observed that the intensity of the emission peak at 355 nm decreases with the appearance of a new emission band 445 nm (ϕ_f = 0.06) (Figure 2f). It is very clear that at higher concentrations of ZrO_2 particles the second emission band at 445 nm dominates over the original BIC emission. It is also interesting to see that with increasing concentration of ZrO_2

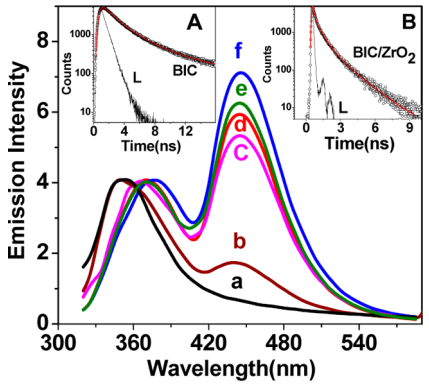

Figure 2. Emission spectra of (a) free baicalein (56 μM) and (b−e) BIC−ZrO_2 complex. Concentrations of ZrO_2 in BIC−ZrO_2 complex are (b) 0.078, (c) 0.625, (d) 1.25, (e) 2.5, and (f) 5 g/L. (Inset) Emission decay trace of (A) BIC in water after exciting at 280 nm and monitoring at 350 nm, (B) BIC−ZrO_2 [[ZrO_2] = 5 g/L]complex in water after exciting at 374 nm and monitoring at 450 nm. L stands for the excitation profile of the laser.

NP the original peak of BIC changes from 355 to 377 nm. However, the second emission peak does not change its position. The second emission band can be attributed to charge-transfer emission.

Earlier we reported CT emission in dye−semiconductor composite materials where TiO_2,[13] ZrO_2,[29,30] and ZnS[32] nanoparticles were used as semiconductor materials. In general, in dye−semiconductor systems, where an electron-transfer reaction takes place from the photoexcited dye to the TiO_2 nanoparticle, the emission intensity of the composite system reduces drastically. Interestingly, it has been observed that the emission quantum yield increases with nanoparticles (ZrO_2) concentration (Figure 2), which includes both pure BIC emission and CT emission. In neat water the BIC molecule has three consecutive OH groups, which can form an intermolecular H bond with bulk water molecules; as a result, nonradiative pathways from photoexcited BIC are more favorable. However, when the molecules adsorb on the ZrO_2 nanoparticle surface or make a complex with ZrO_2 nanoparticles the nonradiative decay of the excited state is less efficient.

On the other hand, when the molecule is adsorbed on the surface, it will be rigidified on the surface, resulting in decrease in internal conversion. As a result, the emission quantum yield of BIC molecules, which does not inject an electron into the nanoparticles, is more than that in the bulk. We also carried out steady-state emission measurements in the BIC−TiO_2 system. BIC emission was completely quenched in the presence of TiO_2 nanoparticles, and no CT emission was observed in the BIC−TiO_2 system.

Here we observed a very interesting feature of the CT emission in the BIC−ZrO_2 complex system. To address the emissive nature of the CT complex, we also carried out time-resolved emission studies in the above systems by exciting pure BIC and BIC−ZrO_2 complex at different wavelengths. In Figure 2 (Inset A) the emission decay trace of BIC in water after exciting at 280 nm and monitoring at 350 nm is shown. The emission decay trace can be fitted multiexponentially with time constants of τ_1 =0.34 ns (69%), τ_2 =2.37 ns (27%), and τ_3 = 9.4 ns (4%) with τ_{av} =1.25 ns. Figure 2 (Inset B) shows the emission decay trace of BIC−ZrO_2 in water after exciting at 374 nm and monitoring at 450 nm. Here we monitored pure CT at

dx.doi.org/10.1021/jp403473h | J. Phys. Chem. C 2013, 117, 17531−17539

450 nm, where the contribution due to pure BIC emission is negligible. The emission decay trace can be fitted multi-exponentially with time constants of τ_1 = 0.09 ns (70%), τ_2 = 0.56 ns (23%), and τ_3 = 1.69 ns (7%) with τ_{av} =0.31 ns. In our earlier investigation we determined the charge recombination (back ET) time by monitoring the CT emission lifetime in coumarin/TiO_2,[13] xanthenes dyes/TiO_2,[42] Qz/ZrO_2,[29,30] and Qz/ZnS[32] systems. It is clearly seen that the lifetime of the CT emission, which indirectly determined the back ET time constant, is too fast to measure by time-resolved emission spectroscopy with subnanosecond time resolution. To understand the charge-transfer dynamics on a shorter time scale it is very important to investigate these processes with femtosecond time resolution. In the next section we carried out transient absorption spectroscopy in both BIC−ZrO_2 and BIC−TiO_2 systems and monitored the charge-transfer dynamics on an ultrafast time scale.

c. Excited-State Dynamics of Free Baicalein. In an earlier section we observed that the emission quantum yield of BIC is very poor and that it also has a shorter emission lifetime. The low quantum yield of emission suggests that a majority of the de-excitation process takes place through a nonradiative transition. To monitor the overall excited-state dynamics of the BIC molecule femtosecond transient absorption spectroscopic measurements have been carried out in acetonitrile, exciting at 400 nm laser light. The solubility of the BIC molecule in water is poor, so to study the excited-state dynamics of free BIC, we chose acetonitrile as a solvent. Figure 3 shows transient

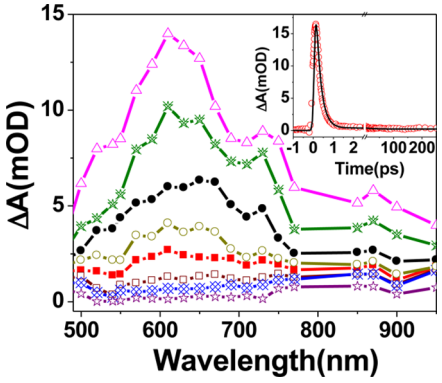

Figure 3. TA spectra of the BIC−ACN system recorded at different time delays (from top to bottom 200 fs, 300 fs, 400 fs, 500 fs, 600 fs, 800 fs, 1 ps, and 20 ps) after exciting at 400 nm laser pulse. (Inset) Transient kinetics monitored at 610 nm.

absorption spectra at different time delays, which consist of broad absorption in the 500−900 nm wavelength range with a transient peak at 610 nm. Transient decay kinetics can be fitted with time constants with τ_1= 250 fs (98.5%), τ_2 = 30 ps (0.6%), and τ_3 > 1 ns (0.9%). Such a comprehensive decay profile is very uncommon among organic sensitizer molecules and can be attributed to the occurrence of a nonradiative decay channel of photoexcited BIC due to the presence of three OH groups. However, it has been observed that the emission life of BIC is 1.25 ns (τ_{av}^{em}), which is quite longer as compared to very fast transient decay kinetics as observed at 610 nm wavelength. This observation clearly indicates that a majority of the de-excitation process takes place through a nonradiative channel. It would be really interesting to monitor the photoexcited behavior of BIC on a semiconductor surface on an ultrafast time scale.

d. Transient Absorption Measurements in BIC−TiO_2 System. Optical absorption studies indicate that BIC forms a strong complex and BIC luminescence is completely quenched in the presence of TiO_2 nanoparticles. This observation clearly suggests that photoexcited BIC injects an electron in the conduction band of the TiO_2 nanoparticle as the process is thermodynamically viable (Scheme 2). To understand the ET

Scheme 2. Mechanistic Scheme of Electron-Transfer and -Trapping for the Coupled Systems Baicalein TiO_2 (Right) and BIC−ZrO_2 (Left)[a]

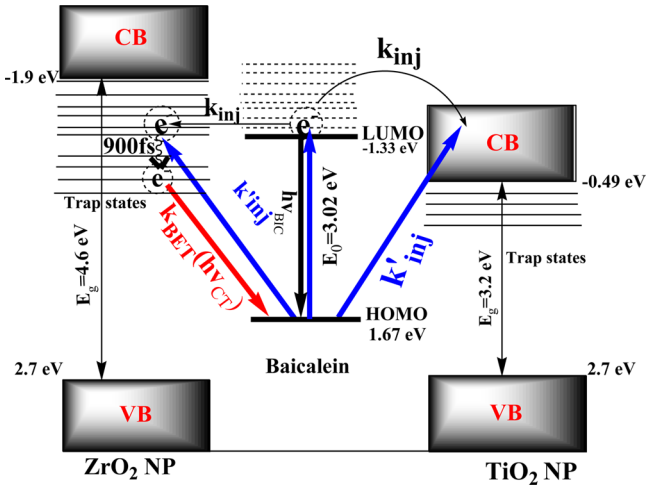

[a]Here LUMO is the excited sensitized dye, k_{BET} is the back-electron-transfer rate, k_{inj} is the electron injection through the excited state, and k'_{inj} is direct electron injection (excitation of CT complex). Energy level with respect to NHE (= normal hydrogen electrode).

dynamics on an ultrafast time scale we carried out femtosecond transient absorption studies after exciting the BIC−TiO_2 system with 400 nm laser light. Figure 4 shows the time-

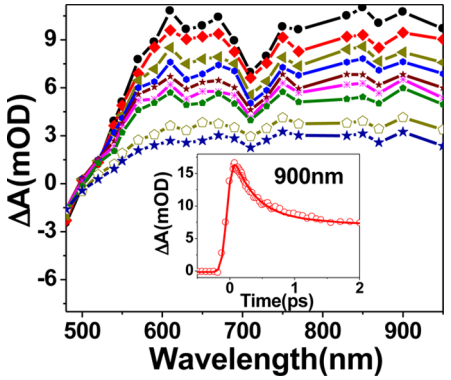

Figure 4. Transient absorption spectra of BIC−TiO_2 complex (from top to bottom 200 fs, 300 fs, 400 fs, 500 fs, 600 fs, 800 fs, 1 ps, 5 ps, and 20 ps) in water at different time delays after 400 nm laser excitation. (Inset) Transient kinetics monitored at 900 nm.

resolved transient absorption spectra of BIC-sensitized TiO_2 nanoparticles in water. The spectrum at each time delay consists of an absorption band with a peak at 650 nm and also a broad absorption band from 700 to 1000 nm. The broad spectral absorption in the 700−1000 nm region is attributed to the conduction band electrons in the nanoparticles (e_{CB}^-).[13−15,21−26] Electron injection time has been monitored

dx.doi.org/10.1021/jp403473h | J. Phys. Chem. C 2013, 117, 17531−17539

Table 1. Life Times of the Transients for BIC−TiO_2 and BIC−ZrO_2 Systems at Different Wavelengths

system	$\lambda_{monitor}$ (nm)	τ_{inj}	τ_1 (A_1%)	τ_2 (A_2%)	τ_3 (A_3%)	τ_4 (A_4%)
BIC−TiO_2	650	<120 fs	350 fs (45%)	6 ps (20.5%)	120 ps (17.7%)	>1 ns (16.8%)
BIC−TiO_2	900	<120 fs	300 fs (52%)	6 ps (23%)	120 ps (10%)	>1 ns (15%)
BIC−ZrO_2	650	<120 fs	5 ps (27%)	100 ps (17%)	>1 ns (56%)	
BIC−ZrO_2	900	<120 fs	900 fs (33%)	10 ps (19%)	100 ps (30%)	>1 ns (18%)

from the appearance of the signal of the BIC cation radical ($BIC^{\bullet+}$) at 650 nm as well as e_{CB}^- at 900 nm and was found to be <120 fs (inset, Figure 4). Assignment of the BIC cation radical ($BIC^{\bullet+}$) has been made on the basis of the results obtained in separate pulse radiolysis experiments, where $BIC^{\bullet+}$ was generated by one-electron oxidation reaction of BIC studied in N_2O-saturated aqueous solution containing 56×10^{-6} mol dm^{-3} BIC dyes and NaN_3 (5×10^{-2} mol dm^{-3}) and is shown in the Supporting Information. Back-electron-transfer dynamics (charge recombination) of the above reaction has been determined by monitoring both $BIC^{\bullet+}$ at 650 nm (Figure 6a) and the electron in the conduction band at 900 nm (Figure 6b). A recombination reaction in BIC−TiO_2 has been found to be a very fast and multiexponential function with time constants of τ_1 = 350 fs (45%), τ_2 = 6 ps (20.5%), τ_3 = 120 ps (17.7%), and τ_4 > 1 ns (16.8%) as monitored at 650 nm (Table 1). Kinetic data at 900 nm have also been fitted multiexponentially with time constants of τ_1 = 300 fs (52%), τ_2 = 6 ps (23%), τ_3 = 120 ps (10%), and τ_4 > 1 ns (15%) (Table 1). The long-time offset (which persists to a delay time of τ > 1 ns of the transients for the BIC−TiO_2 system (Figure 6a and Figure 6b) can be assigned to the slow recombination reaction of the long-lived charge-separated state. This process continues to occur on a nanosecond to microsecond time scale. The slow recombination reaction is due to those electrons, which move to different trap sites with a distribution of trap energy and distance from the adsorbate.[14,42]

e. Transient Absorption Measurements in BIC−ZrO_2 System. Due to its larger band gap and higher conduction band energy level ZrO_2 nanoparticles are used as a noninjecting surface where the excited-state dynamics of dye molecules are monitored.[13,21,43] However, recent studies indicate that electron injection into ZrO_2 nanoparticles is possible by certain photoexcited dye molecules.[27−31] Cyclic voltametry and steady-state luminescence measurements suggest that the energy level of the first photoexcited state (S_1) of the BIC molecule lies below the conduction band level of ZrO_2 nanoparticles. However, steady-state and time-resolved emission studies indicate injection of an electron into ZrO_2 nanoparticles by a photoexcited BIC molecule. To understand the electron-transfer (both electron injection and back ET) dynamics we carried out femtosecond laser spectroscopic experiments on BIC molecules adsorbed on ZrO_2 nanoparticle exciting at 400 nm. Figure 5 shows the time-resolved transient absorption spectra of the BIC−ZrO_2 system in water. The spectrum at each time delay consists of a positive peak at ~650 nm and a broad positive feature in the 750−1000 nm spectral region. The positive peak at 650 nm has been attributed to combination of a cation radical of the BIC molecule (mentioned in an earlier section), and the broad absorption band in the region of 750−1000 nm can be attributed to the injected electron in ZrO_2 nanoparticles. The transient absorption of the BIC−ZrO_2 system in the 450−500 nm region can also be attributed to BIC cation radical (Supporting Information). The peak in the transient absorption spectra that appears at 450−650 nm region

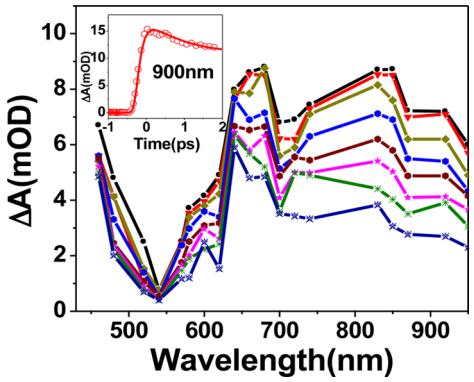

Figure 5. Transient absorption spectra of BIC−ZrO_2 (from top to bottom 500 fs, 1 ps, 2 ps, 5 ps, 10 ps, 20 ps, 50 ps, and 100 ps) complex in water at different time delays after 400 nm laser excitation. (Inset) Transient kinetics monitored at 900 nm.

is due to bleaching of the ground state of the BIC−ZrO_2 system. Since the excited singlet state (S_1) of the BIC molecule is well below the conduction band of ZrO_2 (Scheme 2), the photoexcited BIC molecule will be unable to inject an electron in the conduction band of ZrO_2 nanoparticles. Interestingly, we observed that the transient spectra and kinetics of the BIC−ZrO_2 system are very different compared to those of BIC in acetonitrile; however, it somehow matches closely with the BIC−TiO_2 system. This observation clearly indicates that although the energy level of the photoexcited state of BIC lies below the conduction band of the ZrO_2 nanoparticle still electron injection into the nanoparticles take place. Thus, this injection process can be attributed to injection in the surface states of nanoparticles. The injection process can also be determined by monitoring the appearance time of the injected electron at 900 nm (Inset Figure 5), which was found to be <120 fs. The electron injection process can be described by the following equation

$$ZrO_2 + BIC \Leftrightarrow [ZrO_2{-}BIC]_{complex} \xrightarrow[\text{Electroninjection}]{h\nu} e^-_{SS}(ZrO_2) + BIC^+ \quad (4)$$

Back-ET reaction of the above reaction can be determined by monitoring either the cation radical at 650 nm or the electron in the conduction band at 900 nm (Figure 6B). The kinetic decay trace at 650 nm can be fitted multiexponentially with time constants of τ_1 = 5 ps (27%), τ_2 = 100 ps (17%), and τ_3 > 1 ns (56%). It is interesting to see that the kinetics at 650 nm has a slow component, which recombines in a much longer time scale and can be assigned to the slow recombination reaction of the long-lived charge-separated state, which occurs on a nanosecond to microsecond time scale. Slow recombination reactions are due to the electrons, which are trapped at different trap depths and different distances from the adsorbate, resulting multiexponential dynamics with many slower components. We also monitored the dynamics at 900 nm,

dx.doi.org/10.1021/jp403473h | J. Phys. Chem. C 2013, 117, 17531−17539

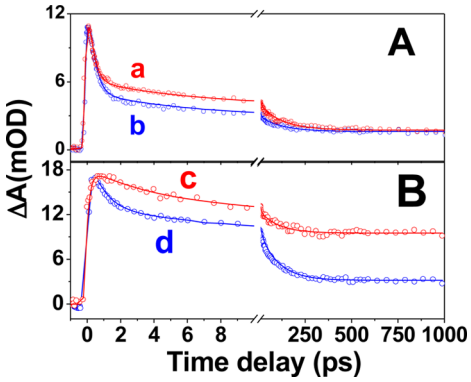

Figure 6. (A) Decay kinetics of (a) cation radical at 650 nm and (b) injected electron at 900 nm in BIC−TiO_2 system. (B) Decay kinetics of (c) cation radical at 650 nm and (d) injected electron at 900 nm in BIC−ZrO_2 system after exciting the samples at 400 nm.

and the kinetic data can be fitted with τ_1 = 0.9 ps (33%), τ_2 = 10 ps (19%), τ_3 = 100 ps (30%), and τ_4 > 1 ns (18.0%). It is interesting to see that kinetic trace at 900 nm decays much faster compared to that at 650 nm. At 900 nm we primarily monitor the injected electron into the nanoparticle, and at 400 nm excitation in the BIC−ZrO_2 system electrons are injected directly into the surface states. Thus, before recombining with the cation radical the injected electron will be going through an electron-trapping process. Thus, the 900 fs component which arises at 900 nm can be attributed to an electron-trapping process in the ZrO_2 nanoparticle (Scheme 2).

f. Surface-State Electron-Transfer and Trapping Dynamics. It is widely reported in the literature that surface states play an important role in any devices made out of semiconductor nanomaterials. It has been reported by us and many other workers that the surface state plays an important and active role in the interfacial electron-transfer reaction. To assess the surface state electron-transfer reaction through the photoexcited state of dye molecules, most of the time ZrO_2 nanoparticles are chosen due to its wide-band-gap and conduction band lying above the LUMO level for most of the dye molecules. Photoexcited molecules like alizarin (Alz) and quinizarin (Qz) could still inject an electron into the surface states due to strong coupling with ZrO_2 nanoparticles through a 6-membered anthraquinone moiety. Interestingly, in all of the above systems electron injection took place through the photoexcited state, where laser excitation (400 nm) primarily excites the molecules and the excited state (S_1 state) of the sensitizers inject an electron (k_{inj}) into the surface states of ZrO_2. However, in the present studies 400 nm laser excitation primarily excites the charge-transfer complex of BIC−ZrO_2 (Figure 1), which on 400 nm laser excitation directly injects an electron (k_{inj}') into the surface states of ZrO_2 nanoparticles. We observed from time-resolved absorption studies that the electron injection time is <120 fs for both TiO_2 and ZrO_2 nanoparticles. Direct excitation of the CT complex facilitates pulse-width-limited electron injection into the surface states. Theoretical calculations carried out by Lego et al.,[44] Wang et al.,[45] Duncan et al.,[46] and Prezhdo et al.[47] suggest a CT mechanism of electron injection in the dye−semiconductor nanoparticle system. It has been suggested that the LUMO in the case of a CT complex is located on the metal center (Ti or Zr) and on excitation the electron gets directly localized on the metal center. Now the localized electron in the metal center diffuses into the conduction band states or surface states of the nanoparticle takes place depending on the semiconductor. It can be seen in Scheme 2 that electron injection in both BIC−TiO_2 and BIC−ZrO_2 systems can take place via photoexcited BIC molecules (k_{inj}) and also direct injection (k_{inj}') to metal centers (Ti or Zr). However, from optical absorption studies (Figure 1) we observed that at 400 nm mostly the CT complex of BIC−MO_2 (M = Ti, Zr) can absorb the laser radiation. Thus, with excitation at 400 nm mostly direct electron injection (k_{inj}') can take place in both systems, where electrons are injected directly into the conduction band of TiO_2 and surface states of ZrO_2 nanoparticles. Electron injection in both systems was found to be pulse-width limited (BET); however, it will be interesting to monitor back-electron-transfer and electron-trapping dynamics in both systems. To observe back-electron-transfer and carrier-trapping dynamics we monitored both the cation radical at 650 nm and the injected electron at 900 nm (Figure 6). Figure 6A shows the kinetics at 650 and 900 nm in the BIC−TiO_2 system, and the data can be fitted multi-exponentially (Table 1), which can be attributed to back-ET dynamics. However, it is interesting to see that the kinetics at 900 nm has a higher contribution of the ultrafast (300 fs) component as compared to that of 650 nm. The extra decay of the transient at 900 nm can be attributed to electron-trapping dynamics in the TiO_2 nanoparticle. However, the kinetics for the BIC−ZrO_2 system at 650 and 900 nm are quite different (Figure 6 B). The kinetics at 900 nm decays much faster with an extra 900 fs component as compared to that of at 650 nm. The extra component can be attributed to electron-trapping dynamics in ZrO_2 nanoparticle. Unlike the TiO_2 nanoparticle system, electrons are injected into the defect states of the ZrO_2 nanoparticle, where trapping dynamics can play a major role. The injected electron can move to different trapping positions like from a shallow trap to deeper trap states. In the present investigation we observed that the BET kinetics in both BIC−TiO_2 and BIC−ZrO_2 systems can be fitted multiexponentially, and it has been observed that the recombination reaction is much slower on the ZrO_2 surface. The strength of the coupling of the dye molecule with both nanoparticles governs the interfacial ET dynamics, both injection and BET. Rego et al.[44] demonstrated charge-transfer dynamics in catechol/TiO_2 nanoclusters after combining ab initio DFT molecular dynamics simulations and quantum dynamics calculations, which suggests that initially charges are localized near Ti^{4+} surface ions which bind with the catechol adsorbate and eventually the charges delocalize through the nanocrystalline material. However, due to the strong coupling back-ET reaction can be facilitated. Wang et al.[45] carried out ultrafast transient absorption studies in a catechol/TiO_2 system where they reported a majority of the injected electrons recombine with the parent cation with a time constant ≈ 400 fs. Similarly, in the present investigation we also observed a 350 fs back-ET time constant in the BIC−TiO_2 system. Interestingly, in the BIC−ZrO_2 system an ultrafast back-ET time constant is absent. Probably in the BIC−ZrO_2 system as the electron are injected directly in the trapped state so the injected electrons can also rapidly delocalize in different trapping positions with a distribution of trap energy and distance from the adsorbate. Earlier Hilgendorff and Sundstrom demonstrated that the distribution of energetically different trap sites for electrons could be responsible for multiexponential kinetics.[42] Similarly, we observed a slow multiexponential recombination reaction with time components from pico- to nanosecond.

dx.doi.org/10.1021/jp403473h | J. Phys. Chem. C 2013, 117, 17531−17539

5. CONCLUSION

We carried out ultrafast transient absorption studies (visible and near IR region) to study interfacial electron-transfer (both electron injection and back-ET) dynamics in baicalein-sensitized TiO_2 and ZrO_2 nanoparticles. Steady-state absorption studies indicated the BIC molecule forms a charge-transfer complex with TiO_2 and ZrO_2 nanoparticles through the pyrogallol and quinone moieties. A new red-shifted charge-transfer emission band was detected in the BIC−ZrO_2 system but not in the BIC−TiO_2 system. Electron injection into the TiO_2 and ZrO_2 nanoparticles has been confirmed by monitoring the cation radical spectra at ∼650 nm and injected electron in the nanoparticles in 750−1000 nm region in real time by transient absorption spectroscopy. The LUMO of BIC lies above the conduction band of TiO_2 but below the conduction band of ZrO_2 nanoparticles, which has been confirmed by combined techniques of steady-state luminescence and cyclic voltametry. The appearance of a cation radical in the transient absorption spectra confirmed that electron injection can take place into the surface states of the ZrO_2 nanoparticle. Electron injection in both nanoparticles takes place in pulse-width-limited (<120 fs) time. After electron injection in ZrO_2 nanoparticles, a majority of the injected electrons move into different trap states (both shallow and deep) with a trapping time of 900 fs. A back-electron-transfer reaction was found to take place much faster in the BIC−TiO_2 system as compared to that in BIC−ZrO_2. The slower back-electron-transfer of the BIC−ZrO_2 system can be attributed to a recombination reaction between the BIC cation radical and the surface-trapped electron (of different trap depth). In the present investigation we observed that strong CT complex formation facilitates electron injection in the surface states of ZrO_2 nanoparticles.

■ ASSOCIATED CONTENT

Ⓢ Supporting Information

High-resolution TEM images of ZrO_2 particle, steady-state optical absorption studies, and BH plot of baicalein in the presence of TiO_2 nanoparticles; transient absorption spectrum of the cation radical of baicalein (uncorrected); steady-state emission spectra of BIC−ZrO_2 complex after exciting at 400 nm; emission decay trace of BIC−ZrO_2 complex after exciting at 400 nm. This material is available free of charge via the Internet at http://pubs.acs.org.

■ AUTHOR INFORMATION

Corresponding Author

*E-mail: hnghosh@barc.gov.in.

Notes

The authors declare no competing financial interest.

■ ACKNOWLEDGMENTS

We thank Dr. Shilpa Tawade Chemistry Division, BARC, for her assistance with cyclic voltammetric measurements. P.M. acknowledges DAE for a research fellowship, and T.D. acknowledges CSIR for a research fellowship. We also thank Dr. D. K. Palit of Bhabha Atomic Research Centre for encouragement.

■ REFERENCES

(1) Miller, R. J. D.; McLendon, G. L.; Nozik, A. J.; Schmickler,W.; Willig, F. *Surface Electron-Transfer Processes*; VCH Publishers, Inc.: New York, 1995.
(2) Memming, R. *Semiconductor Electrochemistry*; Wiley VCH: Weinheim, Germany, 2001.
(3) Kalyanasundaram, K. *Dye-Sensitized Solar Cells*; EPFL Press: Lausanne, Switzerland, 2010.
(4) Kamat, P. V. Meeting the Clean Energy Demand: Nanostructure Architectures for Solar Energy Conversion. *J. Phys. Chem. C* **2007**, *111*, 2834−2860.
(5) O Regan, B.; Grätzel, M. A Low-cost, High-efficiency Solar Cell Based on Dye-sensitized Colloidal TiO_2 Films. *Nature* **1991**, *353*, 737−740.
(6) Alivisatos, A. P. Perspectives on the Physical Chemistry of Semiconductor Nanocrystals. *J. Phys. Chem.* **1996**, *100*, 13226−13239.
(7) Henderson, M. A. A Surface Science Perspective on TiO_2 Photocatalysis. *Surf. Sci. Rep.* **2011**, *66*, 185−297.
(8) Hagfeldt, A.; Boschloo, G.; Sun, L.; Kloo, L.; Pettersson, H. Dye-Sensitized Solar Cells. *Chem. Rev.* **2010**, *110*, 6595−6663.
(9) Listorti, A.; O'Regan, B.; Durrant, J. R. Electron Transfer Dynamics in Dye-Sensitized Solar Cells. *Chem. Mater.* **2011**, *23*, 3381−3399.
(10) Grätzel, M. Solar Energy Conversion by Dye-Sensitized Photovoltaic Cells. *Inorg. Chem.* **2005**, *44*, 6841−6851.
(11) Yella, A.; Lee, H.-W.; Tsao, H. N.; Yi, C.; Chandiran, A. K.; Nazeeruddin, M. K.; Diau, E. W.-G.; Yeh, C.-Y.; Zakeeruddin, S. M.; Grätzel, M. Porphyrin-Sensitized Solar Cells with Cobalt (II/III)-Based Redox Electrolyte Exceed 12% Efficiency. *Science* **2011**, *334*, 629−634.
(12) Tsao, H. N.; Yi, C.; Moehl, T.; Yum, J.-H.; Zakeeruddin, S. M.; Nazeeruddin, M. K.; Grätzel, M. Cyclopentadithiophene Bridged Donor−Acceptor Dyes Achieve High Power Conversion Efficiencies in Dye-Sensitized Solar Cells Based on the tris-Cobalt Bipyridine Redox Couple. *ChemSusChem* **2011**, *4*, 591−594.
(13) Ghosh, H. N. Charge Transfer Emission in Coumarin 343 Sensitized TiO_2 Nanoparticle: A Direct Measurement of Back Electron Transfer. *J. Phys. Chem. B* **1999**, *103*, 10382−10387.
(14) Ramakrishna, G.; Ghosh, H. N.; Singh, A. K.; Palit, D. K.; Mittal, J. P. Dynamics of Back-Electron Transfer Processes of Strongly Coupled Triphenyl Methane Dyes Adsorbed on TiO_2 Nanoparticle Surface as Studied by Fast and Ultrafast Visible Spectroscopy. *J. Phys. Chem. B* **2001**, *105*, 12786−12796.
(15) Benko, G.; Kallionen, J.; Korppi-Tommola, J. E. I.; Yartsev, A. P.; Sundstrom, V. Photoinduced Ultrafast Dye-to-Semiconductor Electron Injection from Nonthermalized and Thermalized Donor States. *J. Am. Chem. Soc.* **2001**, *124*, 489−493.
(16) Moser, J.; Grätzel, M. Photosensitized Electron Injection in Colloidal Semiconductors. *J. Am. Chem. Soc.* **1984**, *106*, 6557−6564.
(17) Kuciauskas, D.; Freund, M. S.; Gray, H. B.; Winkler, J. R.; Lewis, N. S. Electron Transfer Dynamics in Nanocrystalline Titanium Dioxide Solar Cells Sensitized with Ruthenium or Osmium Polypyridyl Complexes. *J. Phys. Chem. B* **2001**, *105*, 392−403.
(18) Ghosh, H. N.; Asbury, J. B.; Lian, T. Direct Observation of Ultrafast Electron Injection from Coumarin 343 to TiO_2 Nanoparticles by Femtosecond Infrared Spectroscopy. *J.Phys. Chem. B* **1998**, *102*, 6482−6486.
(19) Asbury, J. B.; Hao, E.; Wang, Y. Q.; Ghosh, H. N.; Lian, T. Ultrafast Electron Transfer Dynamics from Molecular Adsorbates to Semiconductor Nanocrystalline Thin Films. *J. Phys. Chem. B* **2001**, *105*, 4545−4557.
(20) Haque, S. A.; Tachibana, Y.; Klug, D. R.; Durrant, J. R. Charge Recombination Kinetics in Dye-Sensitized Nanocrystalline Titanium Dioxide Films under Externally Applied Bias. *J. Phys. Chem. B* **1998**, *102*, 1745−1749.
(21) Ramakrishna, G.; Jose, D. A.; Kumar, D. K.; Das, A.; Palit, D. K.; Ghosh, H. N. Strongly Coupled Ruthenium−Polypyridyl Complexes for Efficient Electron Injection in Dye-Sensitized Semiconductor Nanoparticles. *J. Phys. Chem. B* **2005**, *109*, 15445−15453.

(22) Kar, P.; Verma, S.; Das, A.; Ghosh, H. N. Interfacial Electron Transfer Dynamics Involving a New Bis-Thiocyanate Ruthenium(II)−Polypyridyl Complex, Coupled Strongly to Nanocrystalline TiO_2, through a Pendant Catecholate Functionality. *J. Phys. Chem. C* **2009**, *113*, 7970−7977.
(23) Verma, S.; Kar, P.; Das, A.; Palit, D. K.; Ghosh, H. N. The Effect of Heavy Atoms on Photoinduced Electron Injection from Non-thermalized and Thermalized Donor States of MII−Polypyridyl (M = Ru/Os) Complexes to Nanoparticulate TiO_2 Surfaces: An Ultrafast Time-Resolved Absorption Study. *Chem.—Eur. J.* **2010**, *16*, 611−619.
(24) Kar, P.; Verma, S.; Sen, A.; Das, A.; Ganguly, B.; Ghosh, H. N. Sensitization of Nanocrystalline TiO_2 Anchored with Pendant Catechol Functionality Using a New Tetracyanato Ruthenium(II) Polypyridyl Complex. *Inorg. Chem.* **2010**, *49*, 4167−4174.
(25) Verma, S.; Kar, P.; Das, A.; Ghosh, H. N. Efficient Charge Separation in TiO_2 Films Sensitized with Ruthenium(II)−Polypyridyl Complexes: Hole Stabilization by Ligand-Localized Charge-Transfer States. *Chem.—Eur. J.* **2011**, *17*, 1561−1568.
(26) Verma, S.; Ghosh, H. N. Exciton Energy and Charge Transfer in Porphyrin Aggregate/Semiconductor (TiO_2) composites. *J. Phys. Chem. Lett.* **2012**, *3*, 1877−1884.
(27) Huber, R.; Sporlein, S.; Moser, J. E.; Gratzel, M.; Wachtveitl, J. The Role of Surface States in the Ultrafast Photoinduced Electron Transfer from Sensitizing Dye Molecules to Semiconductor Colloids. *J. Phys. Chem B.* **2000**, *104*, 8995−9003.
(28) Ramakrishna, G.; Singh, A. K.; Palit, D. K.; Ghosh, H. N. Dynamics of Interfacial Electron Transfer from Photo-excited Quinizarin (Qz) into the Conduction Band of TiO_2 and Surface States of ZrO_2 Nanoparticles. *J. Phys. Chem. B* **2004**, *108*, 4775−4783.
(29) Ramakrishna, G.; Ghosh, H. N. Determination of Back Electron Transfer Rate from the Surface States of Quinizarin Sensitized ZrO_2 Nanoparticles by Monitoring Charge Transfer Emission. *Langmuir* **2004**, *20*, 7342−7345.
(30) Rath, M. C.; Ramakrishna, G.; Mukherjee, T.; Ghosh, H. N. Electron Injection into the Surface States of ZrO_2 Nanoparticles from Photo-excited Quinizarin and its Derivatives: Effect of Surface-Modification. *J. Phys. Chem. B* **2005**, *109*, 20485−20492.
(31) Verma, S.; Kar, P.; Das, A.; Palit, D. K.; Ghosh, H. N. Interfacial Electron Transfer Dynamics on TiO_2 and ZrO_2 Nanoparticles Surface Sensitized by New Catechol Derivatives of Os(II)-polypyridyl Complexes: Monitoring by Charge Transfer Emission. *J. Phys. Chem. C* **2008**, *112*, 2918−2926.
(32) Rawalekar, S.; Verma, S.; Sreejith, K.; Ghosh, H. N. Interfacial Electron Transfer Dynamics in Quinizarin Sensitized ZnS Nanoparticle: Monitoring Charge Transfer Emission. *Langmuir* **2009**, *25*, 3168−3172.
(33) Greenwald, S.; Rü hle, S.; Shalom, M.; Yahav, S.; Zaban, A. Unpredicted Electron Injection in CdS/CdSe Quantum Dot Sensitized ZrO_2 Solar Cells. *Phys. Chem. Chem. Phys.* **2011**, *13*, 19302−19306.
(34) Nelson, J.; Haque, S. A.; Klug, D. R.; Durrant, J. R. Trap-limited Recombination in Dye-sensitized Nanocrystalline Metal Oxide Electrodes. *Phys. Rev. B* **2001**, *63*, 205321.
(35) Barzykin, A. V.; Tachiya, M. Mechanism of Charge Recombination in Dye-Sensitized Nanocrystalline Semiconductors: Random Flight Model. *J. Phys. Chem. B* **2002**, *106*, 4356−4363.
(36) Kaniyankandy, S.; Rawalekar, S.; Verma, S.; Ghosh, H. N. Charge Carrier Dynamics in Thiol Capped CdTe Quantum Dots. *Phys. Chem. Chem. Phys.* **2010**, *12*, 4210−4216.
(37) Rajh, T.; Chen, L. X.; Lukas, K.; Liu, T.; Thurnauer, M. C.; Teide, D. M. Surface Restructuring of Nanoparticles: An Efficient Route for Ligand-Metal Oxide Crosstalk. *J. Phys. Chem. B* **2002**, *106*, 10543−10552.
(38) Yarwood, J. *Spectroscopy and Structure of Molecular Complexes*; Plenum Press: New York, 1970.
(39) Li, B. Q.; Fu, T.; Gong, W. H.; Dunlop, N.; Kung, H.; Yan, Y.; Kang, J.; Wang, J. M. The Flavonoid Baicalin Exhibits Anti-inflammatory Activity by Binding to Chemokines. *Immunopharmacology* **2000**, *49*, 295−306.
(40) Ikezoe, T.; Chen, S. S.; Heber, D.; Taguchi, H.; Koeffler, H. P. Baicalin is a Major Component of PC-SPES which Inhibits the Proliferation of Human Cancer Cells via a Apoptosis and Cell Cycle Arrest. *Prostate* **2001**, *49*, 285−292.
(41) Lebeau, A.; Esclaire, F.; Rostene, W.; Pelaprat, D. Baicalein Protects Cortical Neurons from Ceta-amyloid (25−35) Induced Toxicity. *Neuroreport* **2001**, *12*, 2199−2202.
(42) Hilgendorff, M.; Sundstrom, V. Dynamics of Electron Injection and Recombination of Dye-Sensitized TiO_2 Particles. *J. Phys. Chem. B* **1998**, *102*, 10505−10514.
(43) Ramakrishna, G.; Ghosh, H. N. Emission from Charge-Transfer State of Xanthene Dye-Sensitized TiO_2 Nanoparticles A New Approach to Determine Back Electron Transfer Rate and Verification of Marcus Inverted Regime. *J. Phys .Chem. B* **2001**, *105*, 7000−7008.
(44) Rego, G. L. S.; Batista, V. S. Quantum Dynamics Simulations of Interfacial Electron Transfer in Sensitized TiO_2 Semiconductors. *J. Am. Chem. Soc.* **2003**, *125*, 7989−7997.
(45) Wang, Y.; Hang, K.; Anderson, N. A.; Lian, T. Comparison of Electron Transfer Dynamics in Molecule-to-Nanoparticle and Intramolecular Charge Transfer Complexes. *J. Phys. Chem. B* **2003**, *107*, 9434−9440.
(46) Duncan, W. R.; Craig, C. E.; Prezhdo, O. V. Time-Domain ab Initio Study of Charge Relaxation and Recombination in Dye-Sensitized TiO_2. *J. Am. Chem. Soc.* **2007**, *129*, 8528−8543.
(47) Prezhdo, O. V.; Duncan, W. R.; Prezhdo, V. V. Photoinduced Electron Dynamics at the Chromophore−semiconductor Interface: A Time-domain *ab initio* Perspective. *Prog. Surf. Sci.* **2009**, *84*, 30−68.